Materials Science and Engineering A 551 (2012) 25–31

Contents lists available at SciVerse ScienceDirect

Materials Science and Engineering A

journal homepage: www.elsevier.com/locate/msea

Dynamic recrystallization and precipitation in low carbon low alloy steel 26NiCrMoV 14-5

Masoud Mirzaee[a], Hamid Keshmiri[a], Golam Reza Ebrahimi[b], Amir Momeni[c,*]

[a] Department of Materials, Mashhad Branch, Islamic Azad University, Mashhad, Iran
[b] Metallurgical and Materials Engineering Department, Ferdowsi University of Mashhad, Mashhad, Iran
[c] Materials Science and Engineering Department, Hamedan University of Technology, Hamedan, Iran

ARTICLE INFO

Article history:
Received 25 February 2012
Received in revised form 13 April 2012
Accepted 17 April 2012
Available online 6 May 2012

Keywords:
Flow curve
Hot deformation
Hot compression
Strain induced precipitation

ABSTRACT

Hot working behavior of 26NiCrMoV 14-5 steel was investigated by performing hot compression testing at a temperature range of 850–1150 °C and strain rates of 0.001–1 s^{-1}. The obtained flow curves at temperatures higher than 1000 °C were typical of dynamic recrystallization, whereas at lower temperatures the flow curves were representing work hardening without any indication of dynamic recrystallization. The apparent activation energy of the material was determined as 437 kJ/mol and the flow stress was correlated to strain rate and temperature using the hyperbolic sine function. The flow curves at high temperatures were successfully modeled using a combination of the Cingara and Avrami equations. However, at temperatures below 1000 °C, the predicted flow curves using the Cingara and Avrami equations were considerably different from the experimental curves. From the low work hardening rates and the increasing of flow stress at temperatures below 1000 °C the possibility of dynamic precipitation could be elucidated. This idea was corroborated by observing the different dependence of flow stress on temperature at low and high temperatures. In order to assess the potential of precipitation in the material stress relaxation tests were performed at low and high temperatures and the results confirmed the possibility of dynamic precipitation at temperatures below 1000 °C.

1. Introduction

Medium carbon low alloy or microalloyed steels are widely used as the hot forged industrial parts. A comprehensive knowledge of the hot working behavior of these alloys including restoration mechanisms, phase transformation and dynamic or static precipitation leads to the more productive design of industrial processing. For this reason, the hot deformation behavior of medium carbon low alloy steels has been the context of several recent papers [1–5]. The greatest concern of the manufacturing engineers involved in the hot forging of these materials is to avoid the flow instability and cracking of the work piece during the hot deformation process. This goal is achieved when the restoration mechanisms of the microstructure, that is, dynamic recovery (DRV) and/or dynamic recrystallization (DRX) occur during hot deformation. These processes actually impede the initiation and the propagation of microcracks which are responsible for the premature fracture [6,7].

To take the advantage of DRV and DRX, hot forging or rolling is often conducted at high temperatures where austenite is the dominant phase. Dynamic recovery in austenite occurs very sluggishly due to its low stacking fault energy (SFE). Therefore, when the accumulative strain energy on account of the build-up of dislocations reaches a critical value, DRX starts [8–10]. Following the work hardening, the softening caused by DRX results in an abrupt decrease in the flow stress and therefore leaves a peak on the flow curve. Although this peak is commonly assumed as the onset of restoration, DRX actually originates from the local bulging of grain boundaries that is initiated at a critical strain (ε_c) 0.6–0.8 times the peak strain (ε_p) [11,12]. Following the peak, the rate of DRX increases up to a maximum and then decreases further until attaining a dynamic balance between work hardening and flow softening. The strain at the onset of the steady state flow (ε_s) along with ε_p is used to characterize a typical flow curve of DRX. A complete understanding about the characteristic strains and the kinetics of DRX for a given material is very essential to a successful design of an actual industrial process. Although the general concept of DRX has been well documented over past decades, the different hot deformation behaviors of the industrial alloys have motivated many recent publications [13–16].

The dynamic or strain induced precipitation of alloying element carbides is another important issue when considering the design of a hot deformation process for a low alloy steels in the austenite region. It is well known that the precipitation of fine carbonitrides

* Corresponding author. Tel.: +98 811 8411403; fax: +98 811 8380520.
E-mail address: ammomeni@aut.ac.ir (A. Momeni).

0921-5093/$ – see front matter © 2012 Elsevier B.V. All rights reserved.
http://dx.doi.org/10.1016/j.msea.2012.04.063

Table 1
Chemical composition of 26NiCrMoV 14-5 medium carbon low alloy steel used in this investigation (wt.%).

C	Si	Mn	S	P	Cr	Mo	Ni	V	N	Fe
0.27	0.2	0.3	0.01	0.01	1.5	0.35	3.7	0.1	0.007	Rem.

in austenite can effectively pin the grain boundaries and inhibit their migration that is required for the initiation of DRX [17–20]. Therefore, the formation of strain induced precipitates (SIP) may delay or inhibit the dynamic softening processes and increase the risk of instabilities. Therefore, to examine the potential of dynamic precipitation in an alloy with strong carbide forming element is very essential to the successful design of an actual hot working process. Hence, the present investigation directed to deal with the study of the hot deformation behavior of medium carbon low alloy 26NiCrMoV 14-5 steel in terms of the constitutive behavior, flow curve prediction and the assessment of the potential of the strain induced precipitation.

2. Experimental procedures

The material used in this investigation was 26NiCrMoV 14-5 medium carbon low alloy steel with chemical composition given in Table 1. The cylindrical specimens with15 mm height and 10 mm diameter were machined from the as-received material according to the ASTM E209 standard. The specimens were reheated for 10 min at 1200 °C and then cooled down to deformation temperature. Graphite was used as the lubricant material to reduce friction and to minimize the barreling of samples during hot compression. The hot compression tests were performed at temperature range of 850–1150 °C and at strain rates of 0.001–1 s^{-1} using a Zwick Roell testing machine equipped with a fully digital and computerized control furnace. Before straining, specimens were soaked for 3 min at deformation temperature. The stress relaxation technique was performed at temperatures of 850 °C, 900 °C and 950 °C after performing a 5% prestrain to analyze the potential of precipitation during hot working.

3. Results and discussion

Fig. 1 shows the representative true stress–strain curves calculated from the load–displacement data at different deformation temperatures and strain rates. Evidently, the obtained flow curves at high temperatures are typical of DRX. The flow curves at high temperatures down to 1000 °C are characterized by a peak after which flow softening brings the curves to the steady state condition. However, at temperatures below 1000 °C, flow stress keeps on an increasing trend to high strains and no indication of DRX is seen. Therefore, the recrystallization stop temperature of the studied alloy may be approximated at about 1000 °C. In addition, it is clearly seen from Fig. 1(b) that at high temperatures, e.g. 1150 °C, both low and high strain rates give rise to the curves showing typical characteristics of DRX. Otherwise at low temperatures, e.g. 900 °C, the flow curves are mostly consisted of a prolonged work hardening region. In order to monitor the influence of deformation temperature on the flow behavior, flow stress at typical strain of 0.4 has been drawn in Fig. 2. Irrespective of strain rate effect, the change in the flow behavior is apparently observed at about 1000 °C. However, this temperature is about 50 °C higher than the T_{nr} reported in the literature for the precipitation of NbC in Nb-bearing HSLA steels [21,22]. This difference may be attributed to the formation of other kinds of carbonitrides likely due to V and Mo.

In order to more address the flow behavior of the material, the apparent activation energy of hot deformation is determined

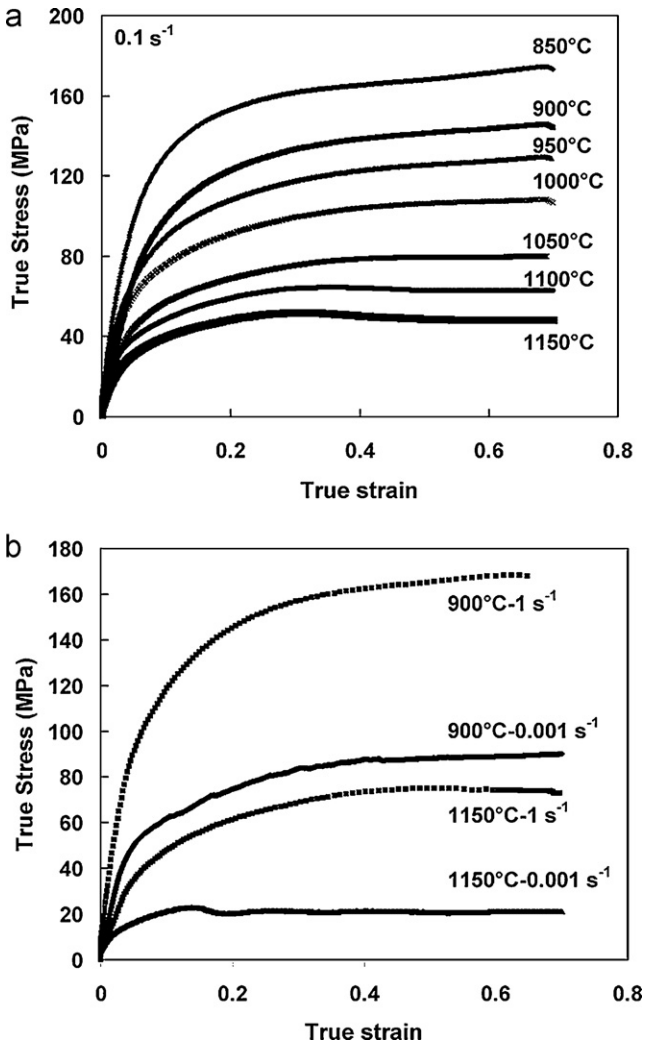

Fig. 1. Representative flow curves obtained at different deformation conditions: (a) strain rate of 0.1 s^{-1} and (b) 900 °C and 1150 °C and strain rates of 0.001 s^{-1} and 1 s^{-1}.

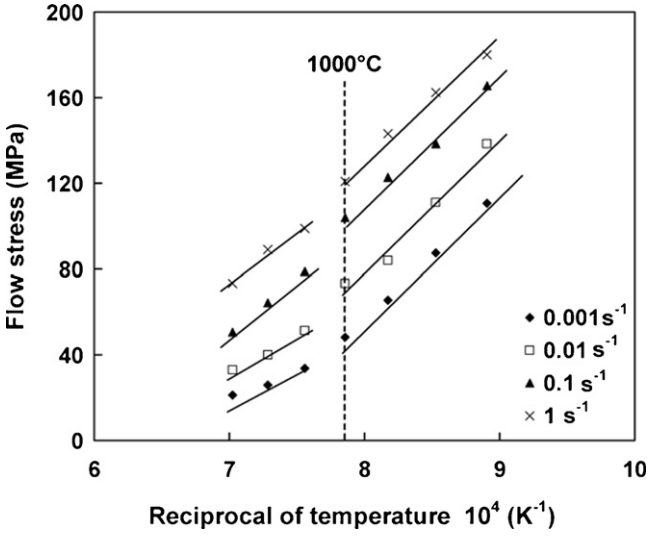

Fig. 2. Flow stress at typical strain of 0.4 as a function of the reciprocal of temperature.

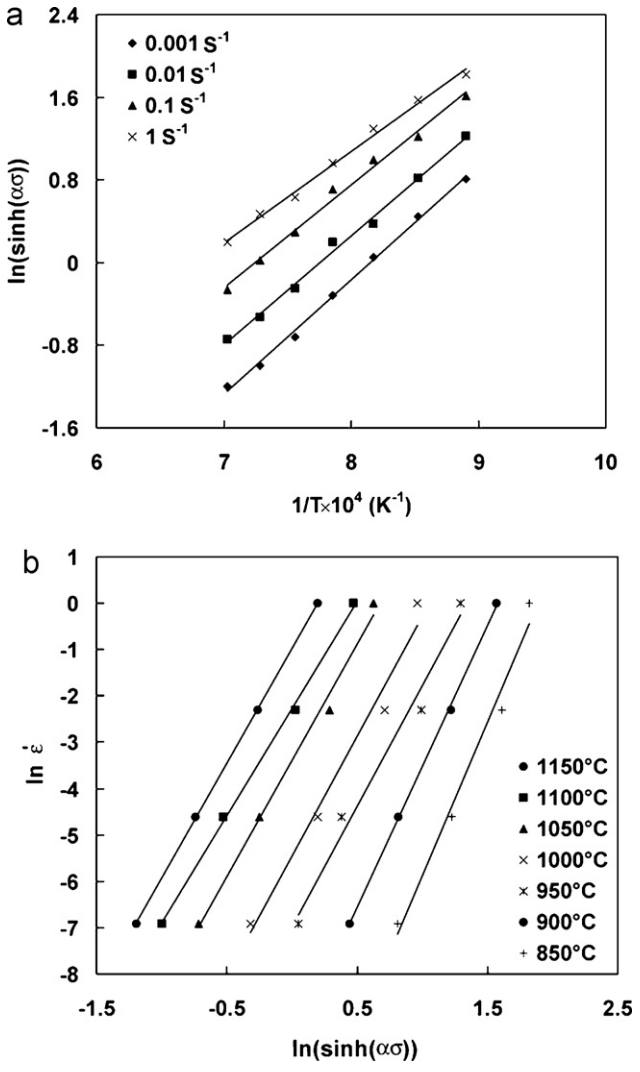

Fig. 3. Variation of the hyperbolic sine function of flow stress versus (a) the reciprocal of deformation temperature and (b) strain rate at the typical strain of 0.4.

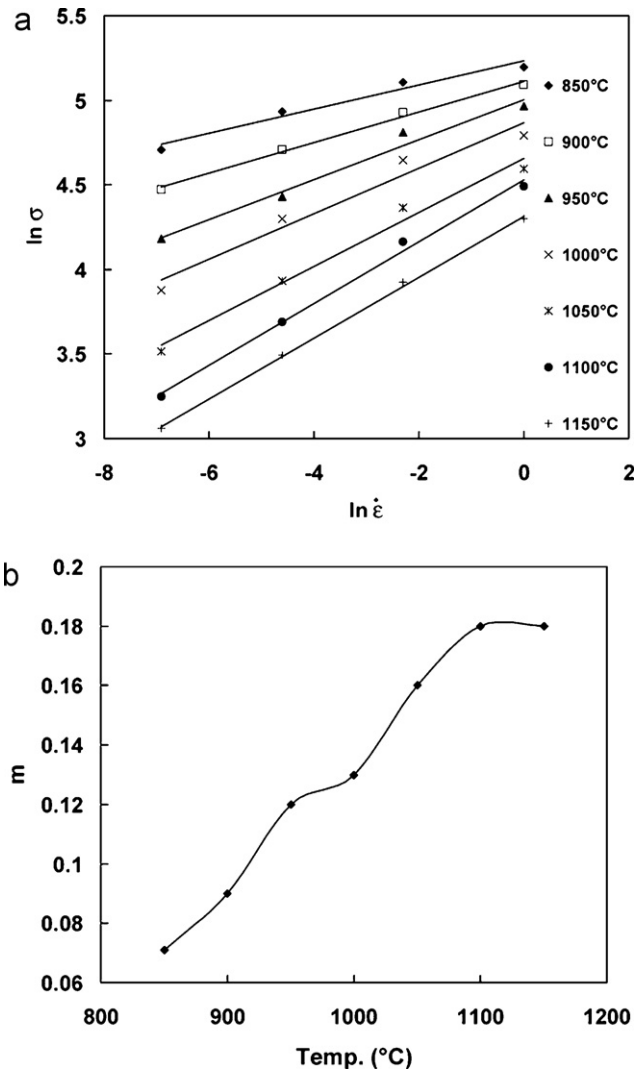

Fig. 4. (a) Flow stress as a function of strain rate in a logarithmic scale for the determination of strain rate sensitivity, m and (b) variation of m with temperature.

through the constitutive analysis. The hyperbolic sine function is widely used under hot working conditions to correlate the flow stress with strain rate and temperature as follows [23]:

$$Z = \dot{\varepsilon}\ \exp\left(\frac{Q}{RT}\right) = A[\sinh(\alpha\sigma)]^n \tag{1}$$

where A, α and n are material constants, Q is the activation energy and Z is the Zener–Hollomon parameter embracing the effects of strain rate and temperature. The partial differentiation of Eq. (1) gives the following description for the activation energy:

$$Q = R\left[\frac{\partial\ \ln\sinh(\alpha\sigma)}{\partial(1/T)}\cdot\frac{\partial\ln\dot{\varepsilon}}{\partial\ln\sinh(\alpha\sigma)}\right] \tag{2}$$

Eq. (2) gives the value of Q from the variations of flow stress with strain rate and temperature according to the hyperbolic sine function. Fig. 3(a) indicates the hyperbolic sine of flow stress as a function of temperature. The average slope of the curves is about 1.12 and is substituted for the first term on the right-hand side of Eq. (2). The second term on the right-hand side of Eq. (2), namely n, is determined as the average slope of the curves in Fig. 3(b). From the least square fitting technique the average value of n is obtained about 4.7. However, n value actually decreases from 6.6 to 4.6 with increasing temperature, reflecting better workability at higher temperatures. It is also worthy of note that the goodness of linear regression at high temperatures (>1000 °C) is better than that in low temperatures (<1000 °C). This is because at high temperatures where DRX is dominant, the flow stress obeys the hyperbolic sine constitutive equation, whereas at low temperatures work hardening is actually dominant.

Substituting the experimentally determined values for the terms in Eq. (2), Q is calculated about 437 kJ/mol. In order to correlate the results with the strain rate sensitivity parameter, m ($= \partial\ln\sigma/\partial\ln\dot{\varepsilon}$), the variation of flow stress with strain rate has been depicted in Fig. 4(a). The results summarized in Fig. 4(b) manifest that m increases considerably as temperature exceeds 1000 °C. This is in agreement with the variation of n with deformation temperature. In fact, the average value of m below 1000 °C is as low as 0.1 while beyond 1000 °C, it reaches over 0.17. This implies that a phenomenon such as precipitation has declined the value of m at temperatures below 1000 °C.

The peak and the onset of steady state deformation are important characteristic points of a typical DRX flow curve. Using the calculated value of Q, the position of these points can be related to the Z parameter. Fig. 5(a) and (b) indicates the dependence of peak strain (ε_p) and stress (σ_p) as well as steady state strain (ε_s) and stress (σ_s) on Z. As expected, DRX is actually shifted to a higher strain and stress as temperature declines or strain rate rises. The proposed equations mentioned in Eqs. (3)–(6) are particularly

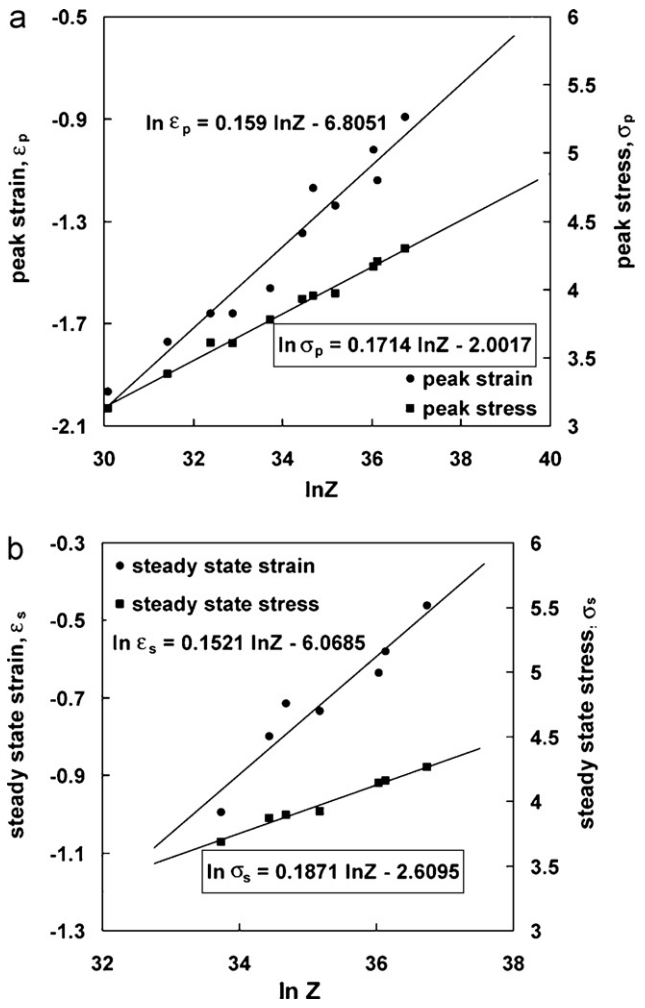

Fig. 5. Variation of (a) peak strain and stress and (b) steady state strain and stress with the Z parameter.

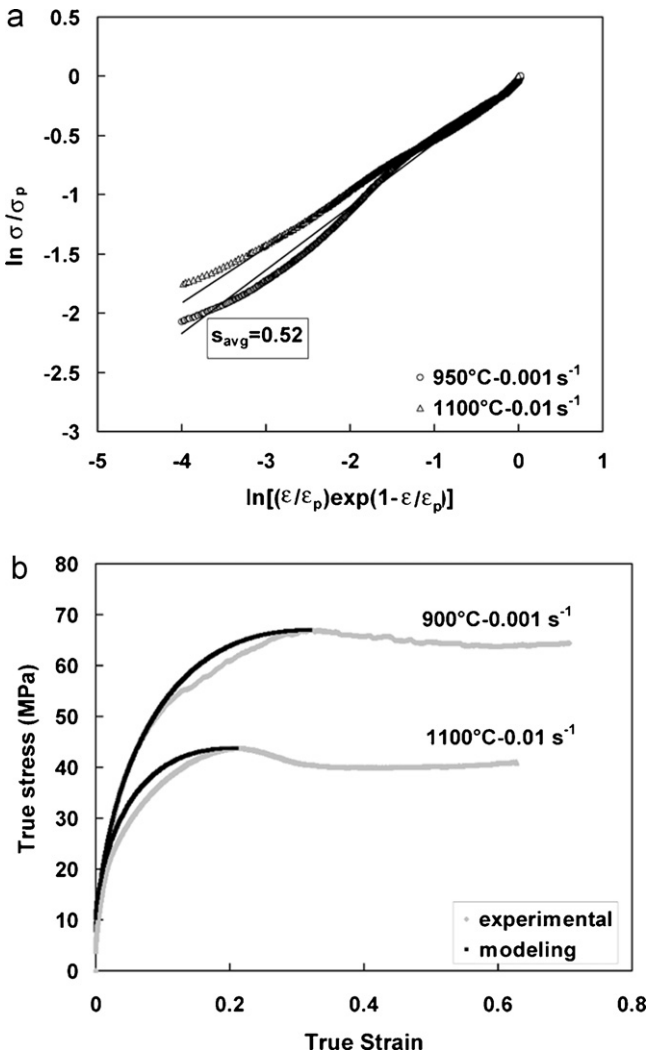

Fig. 6. (a) Fitting of experimental data according to the Cingara equation in a logarithmic scale and (b) experimental modeling of typical DRX flow curves in the work hardening region using the Cingara equation.

useful to generalize the laboratory results to an industrial process where it is essential to have information about the start and finish of DRX:

$$\varepsilon_p = 0.0011Z^{0.159} \tag{3}$$

$$\sigma_p = 0.135Z^{0.1714} \tag{4}$$

$$\varepsilon_s = 0.0023Z^{0.1521} \tag{5}$$

$$\sigma_s = 0.074Z^{0.1871} \tag{6}$$

Moreover, the prediction of flow curve up to the peak will be possible if we know the position of the peak as a function of deformation variables. Different phenomenological or experimental approaches may be used to predict a typical DRX flow curve up to the peak. Here, the method proposed by Cingara and McQueen [24] has been adopted to formulate the flow curve as follows:

$$\frac{\sigma}{\sigma_p} = \left[\left(\frac{\varepsilon}{\varepsilon_p}\right)\exp\left(1-\frac{\varepsilon}{\varepsilon_p}\right)\right]^c \tag{7}$$

where c is a material constant. The value of c is determined as 0.52 from the normalized flow stress-normalized strain plots typically shown in Fig. 6(a). This value is higher than the value of 0.2 reported by Cingara and McQueen [24] for some austenitic stainless steels. The difference may be because of lower work hardening rate and deformation resistance due to the lower alloy content in the studied material comparing to the 300 series stainless steels. Fig. 6(b) indicates that the combination of Eqs. (3), (4) and (7) provides an acceptable accuracy to predict a DRX flow curve up to the peak point. The softening due to DRX following the peak makes it impossible to suggest a single model for the whole flow curve. Previous researchers have used the Avrami equation to describe the kinetics of DRX as well as to model the flow curve between ε_p and ε_s [25–27]. The Avrami equation for modeling a DRX flow curve can be proposed as follows [12]:

$$X_{DRX} = 1 - \exp\left(-0.693\left(\frac{2(\varepsilon-\varepsilon_p)}{\varepsilon_s-\varepsilon_p}\right)^n\right) \tag{8}$$

where X_{DRX} is the fractional softening and n is so-called the Avrami's exponent. X_{DRX} can be interpreted as the flow stress drop from the peak stress with respect to the whole softening $(\sigma_p-\sigma)/(\sigma_p-\sigma_s)$. Substituting this interpretation for X_{DRX} in Eq. (8), a new description is made for $\sigma(\varepsilon)$ between ε_p and ε_s. The average of n value is obtained about 1.8 by plotting $\ln\ln(1/(1-X_{DRX}))$ versus $\ln(2(\varepsilon-\varepsilon_p)/(\varepsilon_s-\varepsilon_p))$ as shown in Fig. 7(a). However, n actually takes a gradual decrease with increasing Z, Fig. 7(b). This is on account of the fact that DRX occurs more slowly at higher strain rates or lower temperatures.

Fig. 8 shows the result of combined Cingara and Avrami model superimposed on the experimental flow curves at the high

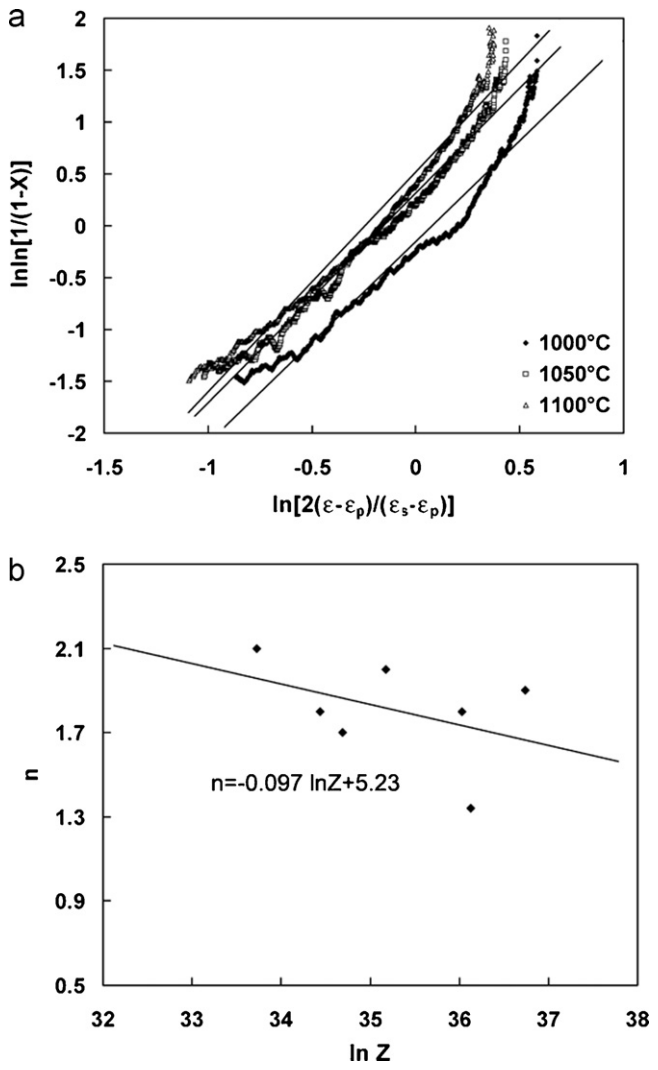

Fig. 7. (a) Avrami plots used to determine the value of n at deformation temperatures of 1000 °C, 1050 °C and 1100 °C and strain rates of 0.01 s^{-1} and (b) variation of n with the Zener–Hollomon parameter.

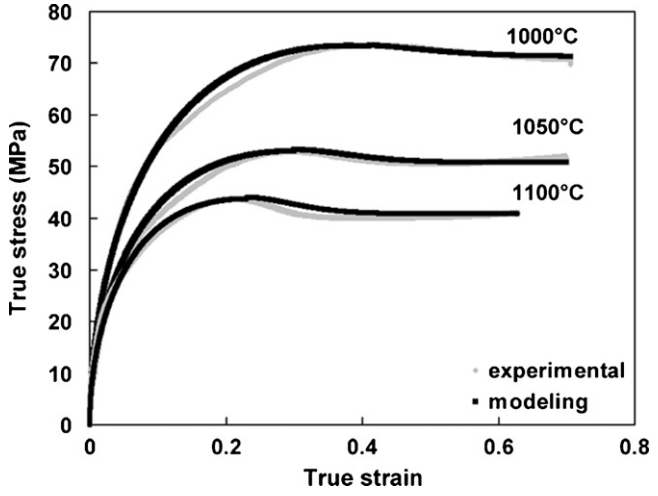

Fig. 8. Combined modeling using Cingara and Avrami equations for the prediction of DRX flow curves at high temperatures and strain rate of 0.01 s^{-1}.

Table 2
Predicted peak strain and stress for the flow curves without DRX peak.

Deformation condition	Peak strain, ε_p	Peak stress, σ_p
850 °C–0.01 s^{-1}	1.32	189.1
900 °C–0.01 s^{-1}	0.67	134.3
950 °C–0.01 s^{-1}	0.5	98
1000 °C–0.1 s^{-1}	0.55	108.9
1050 °C–0.1 s^{-1}	0.43	83.3
1100 °C–1 s^{-1}	0.5	96.4

temperature range (>1000 °C). As a consequence, using the proposed equations one will be able to make an acceptable prediction of the DRX flow curves in the studied alloy. In order to verify this approach at low and high temperatures, the values of ε_p and σ_p are predicted for the flow curves representing only work hardening using Eqs. (3) and (4). Table 2 summarizes the values of ε_p and σ_p for the flow curves without a discernible peak point. These flow curves are modeled in Fig. 9(a) and (b) using Eqs. (7) and (8) and the obtained values for n and c. The position of peak has been indicated by arrows on the flow curves. At very low temperatures, e.g. 850 °C and 900 °C, the peak has been apparently shifted to very high strains. The experimental and modeling flow curves in Fig. 9 indicate that the studied material bear different microstructural phenomena during hot deformation at low and high

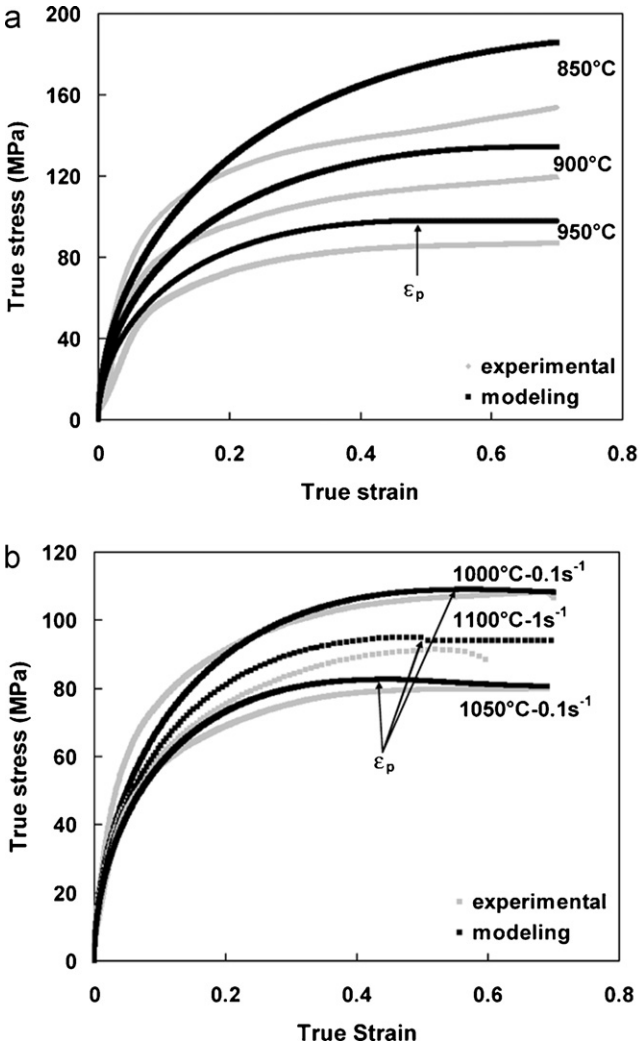

Fig. 9. Combined modeling using Cingara and Avrami equations at (a) low temperatures and strain rate of 0.01 s^{-1} and (b) high temperatures and different strain rates.

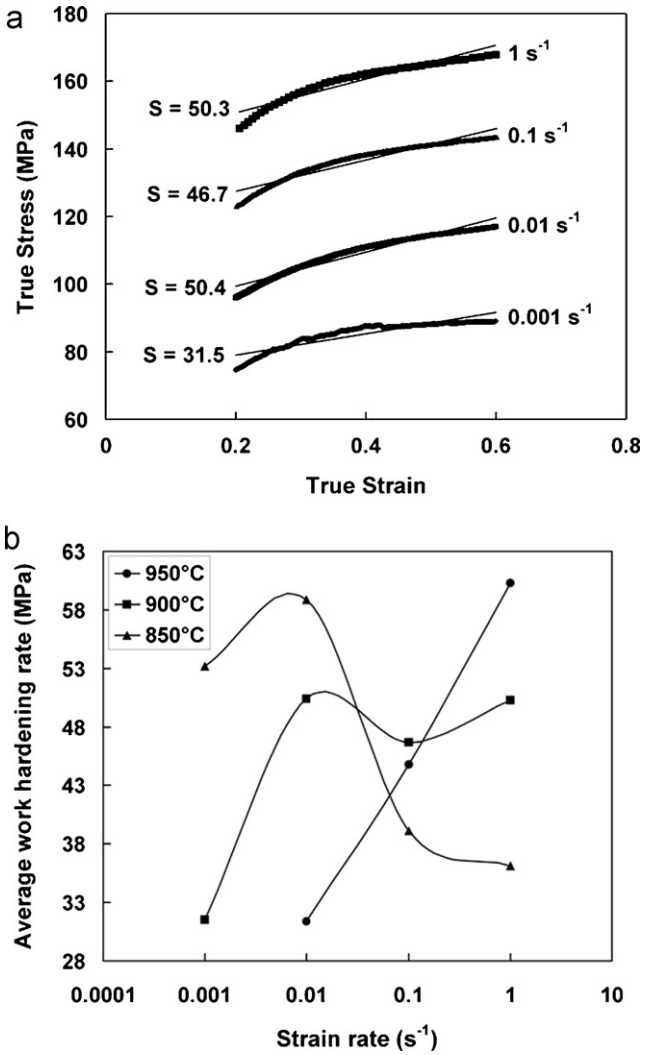

Fig. 10. (a) Determination of the average work hardening rate (θ) at 900 °C in the strain range of 0.2–0.6 and (b) variation of θ with strain rate at 800 °C, 900 °C and 950 °C.

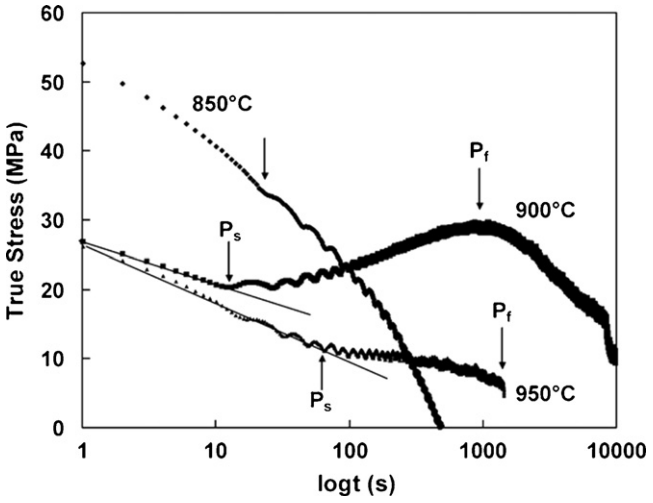

Fig. 11. Stress relaxation plots indicating the potential of strain induced precipitation after a prestrain of 5% at 0.01 s^{-1}. The precipitation start and finish times have been introduced by P_s and P_f, respectively.

temperatures. Although the flow curves selected from the high temperature regime does not contain a discernible peak, but the goodness of modeling seems satisfactory. On the other hand, at temperatures below 1000 °C, the experimental flow curves are very different from the modeling ones. It is worth noting that the work hardening rate in the modeling flow curves are higher than in the corresponding experimental curves. This observation more fortifies the possibility of dynamic precipitation that effectively pins the existing grain boundaries and prevents them from the contribution to the DRX. Instead, sluggish DRV challenges the work hardening and gives rise to the low work hardening.

In order to more discuss the flow behavior at low temperatures, the average work hardening rate was determined using the linear regression of true stress–true strain curve in strain range of 0.2–0.6, as typically shown in Fig. 10(a). The average work hardening rates depicted versus strain rate in Fig. 10(b) indicate abnormal behaviors especially at low strain rates. It is expected that work hardening rate (θ) increases with increasing strain rate. However, the graph indicates that θ increases abruptly at low strain rates (i.e. 0.001 s^{-1} and 0.01 s^{-1}) and then decreases at medium strain rates (i.e. 0.1 s^{-1}). This anomaly can be justified postulating the dynamic precipitation of carbonitrides of alloying elements such as vanadium at low strain rates. At high strain rates, the testing period is too short to form a considerable precipitation. It is important to note that when temperature increases to 950 °C and higher, at low strain rates DRX precedes dynamic precipitation and causes a considerable decrease in the work hardening rate. DRX keeps its upper hand up to the intermediate strain rates, i.e. 0.01–0.1 s^{-1}, and the work hardening rate increases gradually with strain rate as expected. At very high strain rates (i.e. 1 s^{-1} and higher), dynamic precipitation is stimulated and precedes DRX and therefore flow curve is characterized by a high θ value. Referring to Fig. 10(b), the increase in θ with increasing strain rate is more considerable at 900 °C than 850 °C and the abnormal behavior at 950 °C is noticeable at strain rate of 1 s^{-1}. In order to verify the possibility of precipitation during hot deformation of the studied alloy, stress relaxation tests were conducted at 850 °C, 900 °C and 950 °C and the results are drawn in Fig. 11. As it is clearly observed at 850 °C, stress decreases steadily with the time of relaxation. The slope of stress relaxation decreases slightly at the point indicated by an arrow. This can be attributed to the weak interaction of the solute atoms with mobile dislocations giving rise to higher work hardening rate observed in Fig. 10(b). At 900 °C, the stress relaxation curve shows a hardening region between 10 and 1000 s. This hardening behavior is attributable to the strain induced precipitation (SIP) phenomenon. The precipitation start and finish have been indicated by P_s and P_f on the relaxation curves. At 950 °C, the same behavior is observed but at higher times and less hardening influence. Theses results confirm the contribution of dynamic precipitation to the flow behavior of the studied material at low temperatures. The peak of this challenge is around 900 °C and its impact decreases at lower and higher temperatures. Referring to the composition of the studied alloy in Table 1, it is observed that vanadium and molybdenum are potentially able to produce dynamic precipitates with carbon and/or nitrogen. According to the literature, the solubility products of Mo_2C, VC and VN [28,29] are defined as follows:

$$\log[\mathrm{Mo}]^2[\mathrm{C}] = \frac{-7375}{T} + 5 \quad (9a)$$

$$\log[\mathrm{V}][\mathrm{C}] = \frac{-9500}{T} + 6.72 \quad (9b)$$

$$\log[\mathrm{V}][\mathrm{N}] = \frac{-8330}{T} + 3.46 \quad (9c)$$

where [V], [C], [N] and [Mo] are the alloy contents in weight percent and T is the solubility temperature in Kelvin. Using these equations the solubility temperatures of VC, Mo_2C and VN are determined respectively as 865 °C, 873 °C and 980 °C. This assessment indicates

that a cooperation of molybdenum carbide and vanadium carbonitrides is likely to lead the dynamic precipitation and therefore the observed interactions with DRX.

4. Conclusions

Hot working behavior of 26NiCrMoV 14-5 steel was investigated by hot compression and stress relaxation testing. The major results are listed below:

1- At temperatures higher than 1000 °C, DRX was found responsible for flow softening, whereas at lower temperatures the flow curves were associated with work hardening without any indication of DRX.
2- The hyperbolic sine function was used to correlate the flow stress to strain rate and temperature. The value of apparent activation energy of the material was determined as 437 kJ/mol.
3- The DRX flow curves obtained at temperatures higher than 1000 °C were successfully modeled and predicted using a combination of Cingara and Avrami equations. Whereas, below 1000 °C, the models predicted the flow curves considerably different from the experimental ones. This anomalous behavior was attributed to the influence of dynamic precipitation.
4- The stress relaxation tests at low temperatures confirmed the possibility of dynamic precipitation. The lowest times for the start and finish of precipitation were respectively as 10 and 1000 s and were obtained at 900 °C.
5- The solubility products of VC, VN and Mo_2C were calculated using the alloy contents and it was concluded that a combination of V and Mo could cause dynamic precipitation of carbonitrides.

References

[1] X. Lei, W. Cheng-yang, L. Guo-quan, B. Bing-zhe, Trans. Nonferrous Met. Soc. China 19 (2009) 1389–1394.
[2] S. Kim, Y. Lee, D. Lee, Y. Yoo, Mater. Sci. Eng. A 55 (2003) 384–393.
[3] H. Mirzadeh, J.M. Cabrera, J.M. Prado, A. Najafizadeh, Mater. Sci. Eng. A 28 (2011) 3876–3882.
[4] Y.C. Lin, M. Chen, J. Zhong, Mater. Des. 30 (2009) 908–913.
[5] M. Meysami, S.A.A. Akbari Mousavi, Mater. Sci. Eng. A 28 (2011) 3049–3055.
[6] A. Momeni, K. Dehghani, Mater. Sci. Eng. A 528 (2011) 1448–1454.
[7] Y.V.R.K. Prasad, S. Sasidhara (Eds.), Hot Working Guide: A Compendium of Processing Map, ASM International, Materials Park, OH, 1997.
[8] A. Momeni, K. Dehghani, G.R. Ebrahimi, H. Keshmiri, Metall. Mater. Trans. A 41 (2010) 2898–2904.
[9] G.R. Ebrahimi, H. Keshmiri, A. Momeni, M. Mazinani, Mater. Sci. Eng. A 528 (2011) 7488–7493.
[10] S. Mandal, A.K. Bhaduri, V. Subramanya Sarma, Metall. Mater. Trans. A 42 (2011) 1062–1072.
[11] S.I. Kim, Y.C. Yoo, Mater. Sci. Eng. A 311 (2001) 108–113.
[12] A. Momeni, K. Dehghani, G.R. Ebrahimi, J. Alloys Compd. 509 (2011) 9387–9393.
[13] A.H. Meysarni, R. Ghasemzadeh, S.H. Seyedein, M.R. Aboutalebi, R. Ebrahirni, M. Javidani, J. Iron Steel Res. Int. 16 (2009) 47–51.
[14] A. Momeni, K. Dehghani, Metall. Mater. Trans. A 42 (2011) 1925–1932.
[15] J.H. Bianchi, L.P. Karjalainen, J. Mater. Process. Technol. 160 (2005) 267–277.
[16] A. Momeni, S.M. Abbasi, A. Shokuhfar, Can. Metall. Quart. 46 (2007) 189–193.
[17] M. Gómez, L. Rancel, B.J. Fernández, S.F. Medina, Mater. Sci. Eng. A 501 (2009) 188–196.
[18] J. Yang, Q. Liu, D. Sun, X. Li, J. Iron Steel Res. Int. 16 (2009) 75–80.
[19] D. Jorge-Badiola, I. Gutiérrez, Acta Mater. 52 (2004) 333–341.
[20] O. Kwon, A.J. DeArdo, Acta Metall. Mater. 39 (1991) 529–538.
[21] N. Radovic, Mater. Sci. Forum 426–432 (2003) 1553–1558.
[22] A. Momeni, H. Arabi, A. Rezaei, H. Badri, S.M. Abbasi, Mater. Sci. Eng. A 528 (2011) 2158–2163.
[23] C.M. Sellars, W.J. Mc, G. Tegart, Int. Metall. Rev. 17 (1972) 1–10.
[24] A. Cingara, H.J. McQueen, J. Mater. Process. Technol. 36 (1992) 31–42.
[25] J.J. Jonas, X. Quelennec, L. Jiang, E. Martin, Acta Mater. 57 (2009) 2748–2756.
[26] A. Momeni, K. Dehghani, Metall. Mater. Int. 16 (2010) 843–849.
[27] S.I. Kim, Y. Lee, D.L. Lee, Y.C. Yoo, Mater. Sci. Eng. A 55 (2003) 384–393.
[28] M.F. Ashby, K.E. Easterling, Acta Metall. 30 (1982) 1969–1978.
[29] K. Narita, Trans. ISIJ 15 (1975) 145–151.